Atmos. Chem. Phys. Discuss., 15, 4677–4724, 2015
www.atmos-chem-phys-discuss.net/15/4677/2015/
doi:10.5194/acpd-15-4677-2015
© Author(s) 2015. CC Attribution 3.0 License.

Atmospheric Chemistry and Physics Discussions
Open Access

This discussion paper is/has been under review for the journal Atmospheric Chemistry and Physics (ACP). Please refer to the corresponding final paper in ACP if available.

In-situ single submicron particle composition analysis of ice residuals from mountain-top mixed-phase clouds in Central Europe

S. Schmidt[1], J. Schneider[1], T. Klimach[1], S. Mertes[2], L. P. Schenk[2], J. Curtius[3], P. Kupiszewski[4], E. Hammer[4,*], P. Vochezer[5], G. Lloyd[6], M. Ebert[7], K. Kandler[7], S. Weinbruch[7], and S. Borrmann[1,8]

[1]Particle Chemistry Department, Max Planck Institute for Chemistry, 55128 Mainz, Germany
[2]Leibniz Institute for Tropospheric Research, 04318 Leipzig, Germany
[3]Institute for Atmospheric and Environmental Sciences, Goethe-University of Frankfurt am Main, 60438 Frankfurt, Germany
[4]Laboratory of Atmospheric Chemistry, Paul Scherrer Institute, 5232 Villigen, Switzerland
[5]Institute for Meteorology and Climate Research, Karlsruhe Institute of Technology, 76021 Karlsruhe, Germany
[6]School of Earth, Atmospheric & Environmental Science, The University of Manchester, M13 9 PL Manchester, UK

[7]Environmental Mineralogy, Institute of Applied Geoscience, Technical University Darmstadt, 64287 Darmstadt, Germany
[8]Institute for Atmospheric Physics, Johannes Gutenberg University, 55128 Mainz, Germany
[*]now at: Grolimund + Partner AG – environmental engineering, 3018 Bern, Switzerland

Received: 28 November 2014 – Accepted: 27 January 2015 – Published: 19 February 2015

Correspondence to: S. Schmidt (susan.schmidt@mpic.de)

Published by Copernicus Publications on behalf of the European Geosciences Union.

Abstract

This paper presents results from the "INUIT-JFJ/CLACE 2013" field campaign at the high alpine research station Jungfraujoch in January/February 2013. The chemical composition of ice particle residuals (IPR) in a size diameter range of 200–900 nm was measured in orographic, convective and non-convective clouds with a single particle mass spectrometer (ALABAMA) under ambient conditions characterized by temperatures between −28 and −4 °C and wind speed from 0.1 to 21 km h^{-1}. Additionally, background aerosol particles in cloud free air were investigated. The IPR were sampled from mixed-phase clouds with two inlets which selectively extract small ice crystals in-cloud, namely the Counterflow Virtual Impactor (Ice-CVI) and the Ice Selective Inlet (ISI). The IPR as well as the aerosol particles were classified into seven different particle types: (1) black carbon, (2) organic carbon, (3) black carbon internally mixed with organic carbon, (4) minerals, (5) one particle group (termed "BioMinSal") that may contain biological particles, minerals, or salts, (6) industrial metals, and (7) lead containing particles. For any sampled particle population it was determined by means of single particle mass spectrometer how many of the analyzed particles belonged to each of these categories. Accordingly, between 20 and 30 % of the IPR and roughly 42 % of the background particles contained organic carbon. The measured fractions of minerals in the IPR composition varied from 6 to 33 %, while the values for the "BioMinSal" group were between 15 and 29 %. Four percent to 31 % of the IPR contained organic carbon mixed with black carbon. Both inlets delivered similar results of the chemical composition and of the particle size distribution, although lead was found only in the IPR sampled by the Ice-CVI. The results show that the ice particle residual composition varies substantially between different cloud events, which indicates the influence of different meteorological conditions, such as origin of the air masses, temperature and wind speed.

ACPD
15, 4677–4724, 2015

1 Introduction

Ice formation in clouds influences the life-time of clouds and precipitation as well as solar and thermal radiation (Lohmann and Feichter, 2005). There are two major pathways by which ice is formed in the atmosphere: homogeneous and heterogeneous freezing. The spontaneous formation of ice inside droplets at temperatures of lower −37 °C and without any catalysts is called homogenous freezing (Cantrell and Heymsfield, 2005) and occurs in high clouds at a saturation similar to that of liquid water (Koop et al., 2000). Heterogeneous freezing needs particulate catalysts to initiate freezing at temperatures higher than −37 °C in mixed-phase clouds. These catalysts are called ice nucleating particles (INP). There are four different heterogeneous ice formation modes (Pruppacher and Klett, 2010): deposition nucleation, condensation freezing, immersion freezing and contact freezing. Because heterogeneous freezing starts at higher temperatures than homogeneous freezing, ice crystals, which are formed by ice nucleating particles grow faster (by diffusion) and perhaps precipitate first (DeMott et al., 1998).

Ice formation is very selective because of the low number concentration of particles that can act as INP. Roughly about one in 10^5 atmospheric particles can act as INP (Rogers et al., 1998; DeMott et al., 2010). The ice nucleation is induced at some point on the surface of the nucleating particle and the ice nucleation ability of different types if aerosol particles is usually described either by an ice active-site density approach or by classical nucleation theory involving a contact angle (see e.g. Steinke et al., 2014, and references therein). Several laboratory and field studies have shown that certain mineral dusts belong to the most important ice nucleators in the atmosphere (e.g. DeMott, 2003; DeMott et al., 2003; Cantrell and Heymsfield, 2005; Kamphus et al., 2010; Hartmann et al., 2011; Murray et al., 2011, 2012; Hoose and Möhler, 2012; Atkinson et al., 2013; Diehl et al., 2014). Also biological particles like bacteria, pollen and spores (e.g. Diehl et al., 2001; von Blohn et al., 2005; Möhler et al., 2007; Pratt et al., 2009; Prenni et al., 2009; Diehl and Wurzler, 2010), soot (e.g. Cozic et al., 2008a; Pratt and Prather, 2010; Pratt et al., 2010) and effloresced salts (Abbatt et al., 2006;

ACPD
15, 4677–4724, 2015

CC BY

Wise et al., 2012) have good ice nucleation capabilities. There is also some evidence that glassy organics (Froyd et al., 2010; Murray et al., 2010), porous particles (Adler et al., 2013) and lead-containing particles (Cziczo et al., 2009; Ebert et al., 2011) have favorable ice nucleation qualities.

Direct measurements of the chemical composition of single INP or IPR (Ice particle residuals = particles remaining after the ice of cloud ice particles is evaporated) are important to better understand ice formation in mixed-phase clouds, to improve the prediction of precipitation, and to evaluate the influence of anthropogenic aerosol on these processes. Measurements of INP/IPR require instrumentation that can separate the INP/IPR from the background or interstitial aerosol particles and supercooled drops and measure the chemical composition on-line. In several field studies a combination of a CFDC (Continuous Flow Diffusion Chamber; Chen et al., 1998), a CVI (Counterflow Virtual Impactor; Cziczo et al., 2003) which separates the ice crystals from background aerosol and a Single Particle Mass Spectrometer (SMPS; DeMott et al., 2003; Cziczo et al., 2003, 2004; Cziczo, 2004; Pratt et al., 2009; Corbin et al., 2012) to measure ice nucleating particles were deployed. Previous measurements of INP and IPR (on-line and off-line) conducted at the Jungfraujoch showed that particles consisting of mineral components dominate the ice particles number (Kamphus et al., 2010), but also particles containing black carbon (Mertes et al., 2007; Cozic et al., 2008a) and lead (Cziczo et al., 2009; Ebert et al., 2011) were found to be enriched in IPR.

Here we report on measurements conducted with the single particle instrument ALABAMA (Aircraft-based Laser Ablation Aerosol Mass Spectrometer; Brands et al., 2011) to analyze the chemical composition of IPR sampled by two unique different ice sampling inlets. The goal of these measurements was to investigate the chemical composition of IPR in ambient mixed-phase clouds in upward transported boundary layer air and free tropospheric air at the high-alpine research station Jungfraujoch (JFJ; 3580 m a.s.l.) in Central Europe. Additionally, background aerosol was measured by the use of a total inlet during cloud free conditions.

ACPD
15, 4677–4724, 2015

CC BY

2 Experimental

2.1 Measurement location and meteorological conditions

The intensive field campaign INUIT-JFJ/CLACE 2013 in January/February 2013 at the High Alpine Research Station Jungfraujoch (JFJ, Swiss Alps; Sphinx Laboratory, 3580 m a.s.l.; 7°59′2″ E, 46°32′53″ N) took place in the framework of the DFG (Deutsche Forschungsgemeinschaft)-funded research unit INUIT (Ice Nuclei research UnIT) and the Swiss National Science Foundation-funded *Interaction of aerosols with Clouds and Radiation project* (see also overview paper by Schneider et al., this issue). The IPR were sampled out of mixed-phase clouds by the Ice-CVI (Ice Counterflow Virtual Impactor; Mertes et al., 2007) and the ISI (Ice Selective Inlet; Kupiszewski et al., 2014) and fed into the ALABAMA single particle mass spectrometer (Brands et al., 2011). During cloud free times the ALABAMA was connected to the heated total-inlet to sample the background aerosol particles. The Ice-CVI and the total-inlet were located in a central position on the roof of the Sphinx Laboratory and the ISI was located at the railing at the eastern edge of the roof. A short description of the instruments is given in Sects. 2.1 to 2.4. The meteorological conditions during the campaign along with basic information on the encountered cloud types are summarized in Table 1.

2.2 ALABAMA (Aircraft-based Laser ABlation Aerosol MAss spectrometer)

The ALABAMA (Brands et al., 2011) consists of three sections: aerosol inlet, sizing region and desorption/ionization region. The aerosol inlet is an aerodynamic lens (Liu-type; Liu et al., 1995a, b, 2007; Kamphus et al., 2008) which focuses aerosol particles to a narrow beam by utilizing 6 apertures with decreasing diameter. The particles are separated from ambient air and accelerated to 50–100 m s^{-1}, while entering the vacuum-system. For optimal sampling conditions the pressure in front of the aerodynamic lens should be between 0.5 and 5 hPa and for this a critical nozzle is used, which limits the flow to 80 cm^3 min^{-1} under standard working conditions and which re-

ACPD
15, 4677–4724, 2015

CC BY

duces the pre-pressure of the lens to 3.8 hPa. During this campaign, the critical orifice was constructed by a constricted O-ring such that also under Jungfraujoch conditions (ambient pressure around 630 hPa) the lens pressure was regulated to best operating conditions. A skimmer separates the first and the second pumping stages. Two continuous wave detection lasers, which are orthogonal to the particle beam, are located in the second pumping stage. As a modification of the instrument described in Brands et al. (2011), two UV laser diodes (Blu-Ray laser; InGaN, 405 nm) are now used. The particles pass through the laser beams and the scattered light is reflected by an elliptical mirror and detected by a photomultiplier tube (PMT). The vacuum aerodynamic particle size (DeCarlo et al., 2004) can be determined from the velocity of the particles by calibration with particles of known size. In this section the ablation laser (pulsed Nd-YAG-Laser, 266 nm; 6–8 mJ per pulse, 5.2 ns per pulse, max. 21 Hz) is triggered. If one particle passes through both laser beams, the in-house designed and built electronic control system sends out a trigger signal to the ablation laser, the laser shoots and ionizes the particles. The ions are separated in the Z-shaped bipolar time-of-flight mass spectrometer (TOFWERK AG, Switzerland) by their mass-to-charge ratio. In principle both signals (for positive and negative ions) can be detected using a multichannel plate (MCP). However, for this study only positive ions were available due to technical issues. The average mass resolution $m/\Delta m$ of the Z-ToF mass spectrometer ranges between 100 for low m/z values and 200 for larger ions (Brands et al., 2011).

Additionally the particle size distribution was measured by a Sky-OPC (Optical Particle Counter; Grimm 1.129) integrated into the ALABAMA instrument upstream of the aerodynamic lens covering a size diameter range from 0.25 to 52 µm. Due to the size limitation by the inlet system a maximal particle size of approximately 3 µm was measured. Both instruments sampled through 1/4″ stainless steel tubes with different lengths (ISI = 370 cm; Ice-CVI = 126 cm; total = 261 cm). Particle losses inside the sampling tube were calculated with the Particle Loss Calculator (von der Weiden et al., 2009). In the size range between 200 and 500 nm the transmission efficiency is about 99 % for all three inlets. The larger the particles and the longer the tubes, the higher are

ACPD
15, 4677–4724, 2015

CC BY

the losses inside the tubes. For a size of 3 µm the transmission efficiency is between 90 and 45 %. The switching between the three different inlets was performed manually.

2.3 Ice-CVI (Ice Counterflow Virtual Impactor)

The Ice-CVI is designed to sample IPR from mixed-phase clouds. A detailed description and instrumental characterization is provided in Mertes et al. (2007), thus it is only briefly described here. The Ice-CVI uses an omnidirectional inlet, which removes particles larger than 20 µm from the aspired air. The separation of the particles larger than 20 µm out of the sample flow is done with a virtual impactor (VI) downstream of the inlet. After that the supercooled droplets (> 5 µm) are removed by a pre-impactor (PI). The PI consists of impaction plates colder than 0 °C. The supercooled droplets freeze on these plates upon contact while the ice crystals bounce off and remain in the sample flow. Subsequently, a counterflow virtual impactor (CVI, Mertes et al., 2005) rejects the interstitial aerosol particles so that only small ice crystals (i.e. those with aerodynamic size diameters between 5 and 20 µm) remain in the sample flow. It is assumed that such small ice crystals have very recently formed in the close vicinity to the measurement site. For complete sublimation, the small ice particles are injected into particle-free and dry carrier air inside the CVI. The aerosol particles that remain after evaporation/sublimation of the ice are termed IPR. The walls of the evaporation tube as well as the carrier air are at room temperature. The IPR can be transferred to different aerosol instruments for physico-chemical characterization. The sampling principle of the CVI leads to an enrichment of the collected particles. This enrichment (factors between 5 and 10) is given by the ratio of the velocity upstream and downstream the CVI inlet tip.

A CPC (Condensation Particle Counter, model 3010, TSI Inc.) was connected downstream of the Ice-CVI at a suitable position for measuring to determine the total particle number concentration of the IPR. Significant non-zero particle number concentrations indicate the presence of ice particles in mixed-phase clouds.

ACPD
15, 4677–4724, 2015

2.4 ISI (Ice Selective Inlet)

Extracting IPR from mixed-phase clouds was also possible with the ISI (detailed description in Kupiszewski et al., 2014). Small ice crystals (the IPR within are assumed to be representative of the original ice nuclei) are segregated from larger ice crystals, supercooled droplets and interstitial aerosol particles by a combination of four inlet components. The first component is the omnidirectional inlet, which is shielded from above in order prevent large precipitating particles entering the inlet. Subsequently, a custom-made cyclone (BGI Inc.) removes ice crystals, with aerodynamic diameters of ca. 20 µm (D_{50} cut size, i.e., the particle diameter at which 50 % of incoming particles are removed from the sample flow) and larger. Further downstream the removal of supercooled droplets takes place in a custom built ice-coated droplet evaporation chamber using the Wegener–Bergeron–Findeisen process. The key difference to the Ice-CVI is that here the separation of supercooled droplets from ice crystals is conducted in the airborne state via evaporation. Finally, the interstitial aerosol and the cloud condensation nuclei (CCN) released during droplet evaporation are removed by a pumped counterflow virtual impactor ($D_{50} \approx 5$ µm). The extracted ice crystals with aerodynamic diameter between 5 and 20 µm are heated and the released IPR are transferred into the laboratory for physical and chemical characterization using state of the art single particle aerosol instrumentation (single particle soot photometer (SP2), ALABAMA single particle mass spectrometer, Wideband Integrated Bioaerosol Sensor (WIBS) and a Grimm optical particle counter). The ISI additionally allows for simultaneous counting, sizing and imaging of the hydrometers contained in the cloud with the use of two WELAS (white light aerosol spectrometer) aerosol sensor system (Palas GmbH) and a Particle Phase Discriminator (PPD). These are placed behind the cyclone (first WELAS sensor) as well as behind the droplet evaporation unit (second WELAS sensor and PPD). The ISI, together with the downstream aerosol instrumentation, thus provides number size distribution of sampled hydrometers and aerosol particles, infor-

ACPD
15, 4677–4724, 2015

CC BY

mation on ice crystal shape and surface roughness, as well as number size distribution and chemical composition of ice residual particles.

The ISI also enriches the collected particles inside the pumped counterflow virtual impactor with an enrichment factor between 1 and 7.

2.5 Further instruments

Particle Volume Monitor (PVM; Gerber, 1996): The PVM measured the liquid water content (LWC = total liquid water present in a cloud) and the surface area of cloud droplets (e.g., Wendisch, 1998). Cloud droplets cross a laser beam and the scattered light is measured. Elevated LWC values are used to identify cloud events, using a threshold value of 20 $mg\,m^{-3}$. During the measurement campaign two PVMs were operated by PSI (Paul Scherrer Institute) and the University of Manchester.

Cloud Droplet Probe (CDP): The CDP is a forward-scattering spectrometer for determination of particles sizes and concentrations of cloud droplets. Counting and sizing of the particles is done by detecting light scattered by the particles (for more details see for example Lance et al., 2010).

Scanning electron microscopy (SEM): Ice particle residuals (IPR) were collected by a two stage impactor system (50 % cut-off aerodynamic diameters 1.0 and 0.1 µm, respectively) on transmission electron microscopy grids and elemental boron substrates and analyzed by scanning electron microscopy (SEM, FEI Quanta 200 FEG, FEI Eindhoven, the Netherlands) and energy-dispersive X-ray fluorescence (EDX, EDAX, Tilburg, the Netherlands) to characterize the particles with regard to their chemical composition, morphology, size, internal mixing state and electron beam stability (volatility). (For further details see Kandler et al., 2011). Here we only present the size distribution of IPR measured by SEM and compare them to the IPR sizes obtained by the ALABAMA and the sky-OPC. Detailed results on the chemical composition analysis of IPR, INP, and background aerosol by SEM are given in Worringen et al. (2014).

ACPD
15, 4677–4724, 2015

2.6 ALABAMA data evaluation

The data evaluation was done with the software package CRISP (Concise Retrieval of Information from Single Particles; Klimach, 2012) based on the software IGOR Pro (Version 6, WaveMetrics) and following the procedure described in Roth (2014). This software package includes mass calibration, conversion of the mass spectra into "stick" spectra by integration over the peak width, and various procedures to sort the mass spectra into groups or clusters of similar spectra. This sorting can be done manually, by means of cluster algorithms (*fuzzy c-means* or *k-means*), or by searching for certain parameters (e.g., ion signals at a certain m/z ratio).

The Clustering depends to some degree on the interstitial settings of the algorithm and its parameters. The start parameters are *Normalization type and time*, *Preprocessing type*, *Initialisation type*, the *number of clusters* and the *start cluster difference.* Using the *fuzzy c-means* algorithm (e.g. Bezdek et al., 1984; Hinz et al., 1999; Huang et al., 2013) the parameters *fuzzifier* and *fuzzy abort* have to be set accordingly. The cluster parameters are explained in detail in the Appendix.

As only the cations were detected during the INUIT-JFJ/CLACE 2013 campaign the grouping of the clusters into different particle types by using certain marker peaks was difficult in some cases. At the end, seven different particles types were extracted: black carbon (BC), organic carbon (OC), internal mixture of black carbon and organic carbon (BC/OC), lead containing particles, industrial metals, BioMinSal (containing possible bioparticles, minerals or salts), and minerals. The average mass spectra of each particle type are shown in Fig. 1. The association of the mass spectra to the individual particle types is explained in detail below. The error limits of the number of mass spectra per particle types was estimated using counting statistics.

2.6.1 Organic fraction: black carbon (BC) and organic carbon (OC)

The clusters categorized as BC are due to the presence of the typical fragmentation of C_n^+ (Dall'Osto, 2004; Pratt and Prather, 2010) of higher mass-to-charge ratios

ACPD
15, 4677–4724, 2015

CC BY

(see Fig. 1a). In comparison to the black carbon, the organic carbon cluster (Fig. 1b) shows different fragmentations of aromatics ($[C_4H_3]^+$ (m/z 51); $[C_5H_3]^+$ (m/z 63); $[C_6H_5]^+$ (m/z 77); $[C_7H_7]^+$ (m/z 91), Dall'Osto and Harrison, 2006; Pratt and Prather, 2010), amines ($[CHN]^+$ (m/z 27); $[C_3H_8N]^+$ (m/z 58), Pratt and Prather, 2010) or other organic material ($[C_2H_3]^+$ (m/z 27); $[C_3H]^+$ (m/z 37); $[CH_3O/CHNO]^+$ (m/z 43); $[C_4H_2/C_3N]^+$ (m/z 50); $[C_3H_7O]^+$ (m/z 59); $[C_{11}H_{10}/C_8H_{16}NO]^+$ (m/z 142), Pratt and Prather, 2010). Black carbon internally mixed with organic (BC/OC) shows both fragmentation types of $[C_n]^+$ and $[C_nH_mNO]^+$ (Corbin et al., 2012; Fig. 1c).

2.6.2 Lead containing particles

Previous measurements at the Jungfraujoch showed that lead-containing particles can be found in IPR (Cziczo et al., 2009; Ebert et al., 2011). The cluster of lead containing particles shows the typical isotope pattern of lead (m/z 208, 207, 206, 204; Fig. 1d).

2.6.3 Industrial metals

The cluster classified as "industrial metals" (Fig. 1e) shows metal signals from anthropogenic (urban/industrial) emissions like $[Cr]^+$ (m/z 52, 53, 54, 50), $[Co]^+$ (m/z 59), $[V]/[VO]^+$ (m/z 51/67), $[Fe]^+$ (m/z 54, 56), $[Mn]^+$ (m/z 55), $[Ni]^+$ (m/z 58, 60, 61, 62) and $[Zn]^+$ (m/z 64, 66, 68) (De Foy et al., 2012). Chromium and nickel containing particles might also be due to contamination from stainless steel tubes. However, due to no clear evidence of contamination these particles were not excluded from the further analysis.

2.6.4 BioMinSal cluster

The spectra in this cluster type contain only metal cations and can therefore not be unambiguous be assigned to a certain particle type. The spectra in the *BioMinSal* cluster show a mixture or single signals of $[Na]^+$ (m/z 23), $[Al]^+$ (m/z 27), $[K]^+$ (m/z

ACPD
15, 4677–4724, 2015

CC BY

39, 41), $[Ca]^+$ (m/z 40) and/or $[Fe]^+$ (m/z 54, 56). An example of an average spectrum of this particle type is shown in Fig. 1f.

The interpretation of this particle cluster is difficult. The signals are most likely cations of different kinds of salts (Ka_2SO_4 or KNO_3 are more conceivable than sea salt), minerals or primary biological particles, but without corresponding anion an unambiguously assignment to one particle type is not possible. Previous investigations of biological aerosol have shown that metal signals like $[Na]^+$ (m/z 23), $[K]^+$ (m/z 39) or $[Ca]^+$ (m/z 40) dominate the cation spectra (e.g. Fergenson et al., 2004; Pratt and Prather, 2010; Frank et al., 2011). During laboratory studies with test aerosol we also observed mainly single metal signals of sodium and potassium in biological particles, but as well in mineral dust particles. Also iron (Fe^+ m/z 54, 56), which is a typical marker for mineral dust, was observed to occur in some biological particles (maybe due to hemoglobin or due to other ions with an m/z of 56). For these reasons the cluster "BioMinSal" cannot be further differentiated in this study.

2.6.5 Minerals

Typically marker peaks of minerals are: $[Li]^+$ (m/z 6, 7), $[Mg]^+$ (m/z 24, 25), $[Al]^+$ (m/z 27), $[Si]/[SiO]^+$ (m/z 28, 29, 30/44), $[Ca]^+$ (m/z 40), $[Ti]/[TiO]^+$ (m/z 48, 46, 47, 49, 50/64) and/or $[Fe]^+$ (m/z 54, 56) (Trimborn, 2002; Dall'Osto, 2004; Dall'Osto et al., 2010) Clusters containing at least three of the above marker peaks were classified as *minerals* (Fig. 1g).

2.6.6 Others

The cluster *others* includes all particle mass spectra, which are very noisy or could not be unambiguously assigned to any of the above cluster types.

ACPD
15, 4677–4724, 2015

CC BY

3 Results and discussion

During the INUIT-JFJ/CLACE 2013 campaign we measured 71064 background aerosol particles during a measurement time of 217 h and 1808 ice particle residuals during a measurement time of 256 h: 1664 spectra behind the Ice-CVI during 221 h and 144 spectra behind the ISI during 35 h.

3.1 Ice particle residual composition and air mass trajectories

The ALABAMA was used to analyze IPR extracted from mixed-phase clouds by two different inlets: ISI and Ice-CVI. The times during which cloud particles were sampled by the ISI were identified using the cloud liquid water content (LWC)-data measured with two PVM instruments (PSI and University of Manchester) and a CDP (University of Manchester) while the times when the Ice-CVI sampled cloud particles were identified using the ice residual concentration measured with the CPC behind the Ice-CVI. The Ice-CVI cloud events were classified according to the sample efficiency and properties of the Ice-CVI. This classification resulted in (++)-events, where mainly IN were measured; (+−)-events, where the measurements were possibly influenced by secondary ice or contamination by fragments of incoming snowflakes; and (− −)-events, where hardly any ice residuals were detected. The (− −)-events are not included in the following analysis. Table 1 shows the identified cloud events with measurement time, number of acquired mass spectra, event classification and weather conditions and cloud type. The meteorological situation during the whole campaign was mainly influenced by low pressure systems with low temperatures.

The occurrence of artifacts during the measurements using the Ice-CVI as well as the ISI is described in Worringen et al. (2014). Aluminum oxide is an artifact of the measurements with the Ice-CVI and silicon oxide is an artifact of the measurements with the ISI. The impaction plates of the Ice-CVI contain aluminum. When the ice crystals bounce on the impaction plates of the Ice-CVI, some aluminum oxide particles are removed from these plates and can be carried with the air stream to the analysis

ACPD
15, 4677–4724, 2015

CC BY

instrument. The ISI was calibrated with silicon oxide particles, which remained in the system and occurred during the measurements as artifacts. In our dataset it is difficult to distinguish between artifacts and a real component of a particle. Therefore the peaks of m/z 27 (Al^+) and m/z 43 (AlO^+) with respect to the Ice-CVI measurements and the peak of m/z 28 (Si^+) with respect to the ISI measurements were ignored.

In total, we measured 329 spectra during the (++)-events (61 h measurement time) and 1335 spectra during the (+−)-events (160 h measurement time) by using the Ice-CVI. Behind the ISI we measured 144 spectra during 35 h measurement time.

Figure 2 shows the results of the clustering algorithm for all ice particle residual measurements. The Ice-CVI data were analyzed separately for all (++)-events (left pie chart) and for all (+−)-events (middle pie chart). The right pie chart shows the results for all ISI measurements. This analysis shows that the minerals group is one of the dominating fractions in IPR composition measured by using the Ice-CVI during the (+−)-events (21 %) and the ISI (33 %). Interestingly, during the (++)-events minerals represent only a smaller fraction (6 %). We also detected lead containing particles, but only while sampling through the Ice-CVI (12 % in the (++) cases and 11 % in the (+−) cases). During the (++)-events measured behind the Ice-CVI, black carbon internally mixed with organic carbon (31 %) is one of the main fractions. Together with OC (also 31 %), these two particle types represent 62 % of all IPR. It is worth noting that there are more similarities between the Ice-CVI and ISI during (+−)-events than the (++)-events. A reason for that can be that the ISI measurements are also influenced by secondary ice or incoming snowflakes. During the (+−)-events as well as during the ISI-events precipitation occurred. On the other hand, the measurements at the ISI and the Ice-CVI were not done simultaneously, such that also differences in the air mass origin could play a role here.

Backward trajectories were calculated with CRISP (Klimach, 2012) with access to HYSPLIT (Hybrid Single Particle Lagrangian Integrated Trajectory Model, National Oceanic and Atmospheric Administration; Draxler and Rolph, 2012, 2014), which was run using GDAS (Global Data Assimilation System) meteorological dataset. The geo-

ACPD
15, 4677–4724, 2015

CC BY

graphical origin of the air masses and change of altitude during the transport can be used to infer whether the air masses are influenced by surface emissions or mainly characterized by free tropospheric air and long distance transport. During all measurement episodes (total, Ice-CVI, ISI) the air masses approached the measurement station from slightly different directions (Fig. 3). The air masses during the (++)-events came primarily from north-western directions from North America over France and during the (+−)-events additionally more from the North from Scandinavia and Germany. The origin of the air masses during the measurements using the ISI are similar to those of the (++)-events but with a tendency towards southern directions (Fig. 3). During non-cloud episodes air masses approached the measurement location from all directions.

Previous measurements at the JFJ showed that there is an enrichment of mineral dust and black carbon in IPR composition (Mertes et al., 2007; Cozic et al., 2008b; Kamphus et al., 2010). An enrichment of black carbon is not observed in our measurements. Cziczo et al. (2009) found that lead-containing particles are also enriched in the IPR compared to the background aerosol. Our measurements show also that mineral dust (measured behind the ISI and during the (+−)-events) and lead (only measured behind the Ice-CVI) is one of the dominating fractions in the IPR composition. Worringen et al. (2014) report on SEM analyses of particles sampled during the same project behind the ISI and the Ice-CVI. They found lead in two states, namely homogeneous lead-rich particles and small lead inclusions in particles of other material. While the small lead inclusions are not considered as potential artifacts, the large lead-rich particles might be artifacts from mechanical re-suspension of lead containing particles from the surface of the impaction plates of the Ice-CVI. In our case the lead-containing particles are internally mixed with organics, minerals or other metals, therefore we interpret these particles as real atmospheric particles and not as artifacts.

3.2 Event-to-event variability

Figure 4 shows the IPR chemical composition measured during five different events. Although the air masses sampled during all five events have very similar origin and

ACPD
15, 4677–4724, 2015

CC BY

history of altitude (Fig. 5a and b) the chemical composition for each event is different from the others. All air masses during these events arrived rising from a western direction to the measurement platform, such that the chemical composition of these five events was probably influenced by local emissions. During Event 3 and 4 the air masses arrived from a south-western direction. This is reflected in the chemical composition: both events show organic carbon as the main fraction and the amount of lead containing particles is comparable (13 % Event 3 and 15 % Event 4). The differences between Event 3 and 4 are the absence of BC in Event 4 and of minerals in Event 3. The chemical composition of Event 12 is also comparable to Event 4. In this case also the dominating fractions are OC, BioMinSal and minerals. The absence of lead containing particles and presence of 3 % BC in Event 12 are the main differences between Event 12 and Event 4.

Another reason for similarities and differences between these 5 events can be the temperature (Fig. 6). Events 3 and 4 have the highest fraction of OC (nearly 50 % of the particles) and the highest temperatures (Event 3: average temperature $\overline{T} = -7.8\,^{\circ}\mathrm{C}$; Event 4: $\overline{T} = -8.6\,^{\circ}\mathrm{C}$). In contrast to that, Event 12 has the highest amount of minerals and the BioMinSal-type (64 %) and has an average temperature of about $\overline{T} = -17\,^{\circ}\mathrm{C}$. Event 4 has also a high amount of "metal" components (minerals and BioMinSal 38 %) but by closer consideration of the BioMinSal-type it can be shown that this type consists mostly of metal ions together with organic ions in Event 4 and only metal ion signals during Event 12. Therefore the data indicate, that organic material dominates the IPR composition at higher temperatures and metal components from mineral or salty origin dominate at lower temperatures. This finding is surprising, because previous studies found that organics are ice active only at temperatures below $-30\,^{\circ}\mathrm{C}$ (Hoose and Möhler, 2012). However, the organic signal in the mass spectra might also originate from bioparticles, which would explain the ice formation at higher temperatures, because bioparticles have been reported in the literature by many authors to be ice active at higher temperatures as previous measurements show (e.g. Möhler et al., 2008; Hoose and Möhler, 2012). An exception is Event 1. During this event the lowest temperatures

ACPD
15, 4677–4724, 2015

CC BY

($\overline{T}$ = −19.2 °C) of all events prevailed, but a high relative amount of organic components was measured (80 % BC/OC and OC). A reason for this high relative amount of organic material can be local emissions. At this time the total particle data show a short period with high concentrations (> 2000 cm^{-3}, see Fig. 7), which points to local emissions.

3.3 Comparison between background aerosol particle composition and IPR

During non-cloud phases the ALABAMA was connected to the total inlet to measure background aerosol particles. Figure 8 shows the averaged composition of all background aerosol particles along with the IPR composition measured behind the Ice-CVI during the (++)-events and behind the ISI. In comparison to the IPR composition, the measurements show a high fraction of black carbon (18 %; Fig. 8) and only a minor fraction of BC/OC (4 %). The fraction of the particle type "BC/OC" in the background aerosol is comparable to that in the IPR sampled by the ISI. However, also the aerosol particles are dominated by the particle types "organic carbon" (42 %) and "BioMinSal" (30 %). Previous high mountain-top measurements at the Storm Peak Laboratory (SPL; 3200 m a.s.l.) in northern Colorado show also organic as the major component in the background aerosol (DeMott et al., 2003; Cziczo, 2004). The differences as compared to the IPR compositions are the negligibly small amount (< 0.1 %) of lead-containing particles and the much smaller amount of minerals (about 1 %) than observed in the IPR. This is partly in contrast to other measurements. Previous measurements with the ATOFMS at the Jungfraujoch as well as airborne measurements over North America show 5 and 10 % lead-containing particles in the background aerosol (Murphy et al., 2007) but also only a small amount of mineral dust or fly ash measured at the Storm Peak Laboratory (DeMott et al., 2003).

Previous investigations show that the presence of a high potassium peak in the mass spectra in combination with organic carbon is a marker for biomass burning (e.g. Pratt and Prather, 2010; Twohy et al., 2010; Corbin et al., 2012) or biogenic aerosol (e.g.

ACPD
15, 4677–4724, 2015

CC BY

Trimborn, 2002; Pratt and Prather, 2010). Closer consideration of the three different carbon clusters (BC, BC/OC, OC) shows that potassium is present in nearly every mass spectrum. In the background aerosol 45282 mass spectra including black or organic carbon were measured: 92 % of all these mass spectra show potassium. The BC-type includes the mass spectra without potassium (20 %; only 1 % in the OC/BC-type and 6 % in the OC-type). The same observation holds for the IPR composition: the particle types including organic carbon measured by the use of the Ice-CVI as well as the ISI show more spectra including potassium (94 % of all OC and OC/BC spectra while using the Ice-CVI and 98 % while using the ISI). Because of these results spectra with a potassium peak cannot clearly be assigned to biomass burning or biological particles.

3.4 Influence of the air mass trajectories on the aerosol composition

The chemical composition of the background (out-of-cloud) aerosol has been shown in Fig. 8. The high variability of the measured IPR might be due to the different aerosol properties when air masses arrive from different geographic origin and/or different altitudes at the Jungfraujoch. Therefore, we investigate here how air masses origin influences the aerosol properties. Because of the saddle position of the JFJ, there are only two possibilities of how the air masses can approach the measurement platform (Fig. 6). Predominantly, the air masses arrive from northwestern direction over the Swiss plateau (wind direction of approx. 315°). Less frequently, the approach was from a southeastern direction from the inner Alps (approx. 135°, via the Aletsch Glacier). According to the direction from which air masses approach the measurement platform, the chemical composition is influenced predominantly by anthropogenic and organic emissions or by mineral dust sources. To assess the influence of origin and the average altitude of the air masses during their transport to the Jungfraujoch, we compare two time periods with aerosol measurements using the total inlet (11 February and 19 February 2013). The chosen time periods exhibit nearly the same relative humidity, potential wet bulb temperature and temperature (Fig. 6).

ACPD
15, 4677–4724, 2015

CC BY

Figure 9 shows the chemical composition of the aerosol particles for both time periods, along with corresponding back-trajectories. The comparison shows that more particles containing BC (internally mixed with ammonium or the BioMinSal-type) and the BioMinSal-type are observed in the air masses arriving from a northwestern direction (19 February 2013), while the measurements during the SE-event show more OC containing particles (internally mixed with ammonium or the BioMinSal-type). The fraction of particles measured containing only potassium and pure organic carbon is very similar for both events.

The air masses not only approached locally from different directions, but also had different long-range origins (see back trajectories Fig. 9). The air masses measured on 19 February 2013 (NW-event) approached from the north over Germany. The chemical composition of the measured particles is dominated by black carbon internally mixed with ammonium and the BioMinSal-type. In contrast to the 19 February 2013, the air masses on 11 February 2013 that also originated mostly from the North but approached over southern France, and from southern Europe (western Po Valley) contain higher amounts of OC and BioMinSal containing particles. The vertical transport pathway of the air masses could be an indicator for a local, anthropogenic influence on chemical composition. In contrast to the air masses from the north-western direction the air masses from the southeast have been lifted from low altitudes, thereby bringing anthropogenic emissions (e.g., from the Po Valley) up to the altitude of the measurement station. The air masses from the north-western direction stayed nearly at the same altitude for the last three days prior to the measurement.

3.5 Size distribution of IPR and background aerosol

Ice-CVI and ISI both extract small ice particles in the size range from 5 to 20 µm from mixed-phase clouds (Mertes et al., 2007; Kupiszewski et al., 2014) while the upper cut-off of the total inlet was 40 µm for wind speeds up to 20 m s^{-1} (Weingartner et al., 1999). Figure 10 shows the size distributions of IPR measured with the ALABAMA (a, c, e) and the Sky-OPC (b, d, f) compared with ESEM measurements (a–d). Figure 10a

ACPD
15, 4677–4724, 2015

CC BY

shows the size distributions of IPR measured by ALABAMA and ESEM applying the Ice-CVI. Figure 10c the size distributions measured by ALABAMA and ESEM using the ISI. In Fig. 10b and d, the corresponding size distributions measured with the Sky-OPC are shown. Figure 10e and f shows the size distribution measured by ALABAMA and the Sky-OPC using the total inlet. The measurement times for Ice-CVI and ISI are given in Table 1; the measurements using the total inlet were done during all cloud-free periods. For all three inlets (total, Ice-CVI, ISI) the maximum of the detected IPR measured with the ALABAMA and also with the Sky-OPC is in the size range of 300–650 nm. The IPR size distributions measured by ALABAMA and SEM behind the Ice-CVI are in very good agreement (Fig. 10a). In contrast, the IPR size distribution measured behind the ISI are somewhat different. (Fig. 10c): both distributions show two maxima, but the positions of the maxima are not the same. The ALABAMA IPR distribution has a primary maximum in the size bin 0.4–0.5 µm and a secondary maximum in the size bin 1.3–1.6 µm. The SEM IPR distribution both maxima are shifted to larger sizes. The first maximum is in the 1–1.5 µm interval and the second maximum is in the 2–2.5 µm interval. However, total count rates are very low, so this difference should not be overemphasized. Furthermore, SEM measures geometric diameters, while the sizes determined by ALABAMA refer to the vacuum aerodynamic diameter. In contrast to the size distribution measured with the ALABAMA and ESEM, the size distribution measured with Sky-OPC does not show a maximum but only a decreasing number concentration of particles with increasing particle diameter from 100 to 500 nm. This difference is a result of the detection efficiency of the ALABAMA and ESEM, which is the highest around 400 nm. Figure 10f shows that the background aerosol particles have a size range of up to approximately 20 µm with a higher number of smaller particles (< 1 µm). The relative amount of larger particles is (d > 1 µm) clearly elevated for the ice residuals, both behind the ISI and Ice-CVI (Fig. 10b and d). Note that the measurements of background particles (out of cloud) and IPR were conducted by definition at different times, such that the absolute amount of particles cannot be compared.

ACPD
15, 4677–4724, 2015

CC BY

As mentioned above, relatively more IPR larger than 1 µm were observed compared to the background aerosol particles. The percentage of the background aerosol particles larger than 1 µm (vacuum aerodynamic diameter) measured by ALABAMA was only 3 %, while 10–19 % of the IPR behind the Ice-CVI and ISI were larger than 1 µm. Therefore, the chemical composition of these particles has been analyzed separately:

Figure 11 shows the chemical composition of the IPR and background aerosol particles larger than 1 µm. The IPR larger than 1 µm measured behind the Ice-CVI are dominated by minerals, OC (also mixed with BC) and the BioMinSal-type, but lead containing particles are found to a similar percentage (15 %) as in all IPR (12 %, see Figs. 2 and 8). OC is the main fraction of the particles larger than 1 µm measured behind the ISI. In the background aerosol supermicron particles are dominated by the BioMinSal-type. The finding that the BioMinSal-cluster is one of the major components the IPR as well as the background aerosol for $d > 1$ µm strengthens the assumption that the metal ions detected in these mass spectra are likely metal cations of primary aerosols like sea salt, minerals or biological particles, which are mainly found in the coarse mode (Seinfeld and Pandis, 2006).

The size distribution allow also for an estimation of the ice active site (e.g., Vali, 2008) density of particles larger than 1 µm compared to those smaller than 1 µm: assuming that each IPR corresponds to at least one ice active site on the original aerosol particle (otherwise it would not have acted as an INP), we can estimate the ice active site density for the particles analyzed by ALABAMA, separated for particles smaller than 1 µm and larger than 1 µm. The number of ice active sites per IPR surface (ice active site density) is 2.0×10^{-7} nm^{-2} for $d > 1$ µm and 1.6×10^{-6} nm^{-2} for particles with $d < 1$ µm. Relating the number of ice active sites to the total aerosol surface yields 7.1×10^{-10} nm^{-2} for $d > 1$ µm and 4.3×10^{-9} nm^{-2} for $d < 1$ µm. In both cases the ice active site density is larger for particles smaller than 1 µm. This is an important finding and explains the high number of IPR found in the size range below 1 µm. However, it should be noted that the assumption that each IPR corresponds to one ice active site may underestimate the number of ice active sites. In cases where more than one ice active

ACPD
15, 4677–4724, 2015

site is found on the particles, also only one ice crystal will form and one IPR will remain. Thus the estimated number yields a lower limit for the ice active sites.

4 Summary and conclusions

This paper presents results of the single particle measurements during the INUIT-JFJ/CLACE 2013 campaign conducted at the Jungfraujoch in January/February 2013. In agreement with previous measurements at the Jungfraujoch (Chou et al., 2011; Kamphus et al., 2010; Mertes et al., 2007), it was found that larger particles are more efficient ice nuclei. Specific analysis of only those particles > 1 µm showed that the chemical composition of these larger particles is dominated by organic material and the "BioMinSal" type, both in the IPR as well as in the background aerosol. Besides, the "minerals" group was indicated as one of the main fractions in the IPR composition measured behind the Ice-CVI. From the finding that IPR have a higher relative number of larger particles than the background aerosol particles we conclude and confirm a better ice nucleation ability for the larger, primary aerosol particles such as minerals, salt and biological particles.

In general, IPR are enriched in organic material, partly also internally mixed with BC. Additionally, minerals and lead were found in IPR as has already been observed in previous measurements conducted at the JFJ (Mertes et al., 2007; Cozic et al., 2008b; Cziczo et al., 2009; Kamphus et al., 2010; Ebert et al., 2011). In comparison to the composition of the IPR measured using the Ice-CVI, the measured composition using the ISI is dominated by minerals, and no lead containing particles were found, while 12 % of the IPR sampled using the Ice-CVI included lead. In contrast to Cozic et al. (2008) we found no enrichment of pure black carbon in the IPR composition. Only the chemical composition of the background aerosol particles shows a high fraction of black carbon. These results comply with previous investigations (DeMott et al., 1999; Dymarska et al., 2006; Hoose and Möhler, 2012) describing black carbon as a good ice nuclei but only at lower temperatures and its ice nucleating ability appears to be

ACPD
15, 4677–4724, 2015

CC BY

reduced if coatings by organic material or sulfuric acid are present. During the INUIT-JFJ/CLACE 2013 campaign the temperatures were never lower than −30 °C; see Fig. 6. In the background aerosol, the main particle fraction is also organic carbon. The high amount of organic material in the background aerosol as well as in the IPR motivates further investigation of different organic material by single particle mass spectrometry to better characterize the organic fraction. While there have been previous observations that organic matter is of general importance for ice nucleation ability (DeMott et al., 2003; Cziczo et al., 2004), recent laboratory studies have shown the importance of porous and glassy organic matter for ice nucleation (Murray et al., 2010; Adler et al., 2013).

The investigation of the influence of the temperature and the origin and altitude of the air masses on the chemical composition of IPR and aerosol particles indicate that organic material dominates the IPR composition at higher temperatures and metal components from mineral or salt at lower temperatures which is in contrast to previous findings (e.g. Möhler et al., 2008; Hoose and Möhler, 2012). It was illustrated that the origin (geographic and altitude) of the air masses influenced the chemical composition of the aerosol particles. For the non-cloud aerosol, the particles sampled in air masses characterized by free tropospheric air and long distance transport were found to be dominated by BC and single metal ions from salt, mineral or biological sources (BioMinSal-type). These particle types were probably partly mixed with secondary inorganic components, because NH_4^+ was detected in some spectra. In contrast to that, the particles in air masses which are influenced by surface emissions are dominated by organic carbon and potassium.

Appendix A: Parameters underlying the clustering algorithm

This section describes the cluster parameters of the software package CRISP. The chosen parameters are listed in Table A.

ACPD
15, 4677–4724, 2015

A1 Normalization type and time

To compensate for differences in the ionization efficiency, each mass spectrum is normalized to the sum of the signal intensities with preservation of the relative relationship of the signals. By this, the influence of absolute signal intensity is decreased. Absolute signal intensity is not needed because the laser ablation method does not measure quantitatively. The point at which the normalization is applied in the analysis sequence can be chosen. In case of measuring both polarities the spectra of both polarities are first merged, and normalization can be applied before, after or before and after concatenation.

A2 Preprocessing type

Preprocessing (before normalization) can be applied to increase mass signals with lower intensity with respect to signals with a higher intensity, such that the presence of a certain m/z has more significance than the signal intensity in the calculation of the distance to the reference spectrum. Typically the square root of the signal intensities is used.

A3 Initialisation type

This parameter defines the way the reference mass spectra are selected. Two options are available:

- *find different startcluster*: different spectra are randomly selected according to certain criteria
- *random*: reference spectra are chosen randomly

Reference spectra can also be determined manually, however, this last option is not very useful for field data because the number of particle types is unknown.

ACPD
15, 4677–4724, 2015

CC BY

A4 Number of cluster

The result of the clustering is highly dependent on the pre-selected number of clusters. In the case that the number of clusters is too small, some cluster types cannot be found, while in the case that the number is too large, too many similar spectra are assigned to different clusters. In the fuzzy c-means algorithm all non-matched spectra are collected in a rest cluster.

A5 Cluster difference

This parameter determines the distance between the spectra which are chosen as start references at "find different startcluster". The *cluster difference* is between 1 and 0, whereby a *cluster difference* of 1 means that the chosen startclusters are identically. This distance results from the Pearson correlation and affects the number of the resulting clusters. The number of clusters increases with increasing similarity of the references and is constant at a value of 0.7 (Roth, 2014). If the *cluster difference* is too small, the distinctions between the clusters are too large, resulting in too few cluster types. Thus, it is recommended to use more similar reference mass spectra and to summarize those clusters that show similar mass spectra at the end of the clustering.

A6 Fuzzifier and fuzzy abort

The *fuzzifier* (also called *fuzzy weighting* exponent) is a dimension of fuzziness of the classification of the cluster ($1 \leq fuzzifier \leq 8$; e.g. Huang et al., 2012). The bigger the *fuzzifier*, the more inaccurate is the assignment to the references, because the spectra cannot exactly be assigned to one cluster. The distance d_{ij} between spectra i and reference j is weighted with:

$$d_{ij}^{\frac{1}{z-1}} \tag{A1}$$

ACPD
15, 4677–4724, 2015

CC BY

where z is the *fuzzifier*. When the preprocessing option of CRISP is used, it has been found that the result of the clustering is independent of the *fuzzifier* value (Roth, 2014).

During the clustering, each mass spectrum is compared to the reference spectra in terms of distance, membership and correlation. If these parameters fulfill the preselected criteria, the mass spectrum is sorted into the cluster represented by the reference and the average spectrum is calculated again. Subsequently all mass spectra are compared again with the reference spectra. This procedure is repeated until the criterion of abort (*fuzzy abort*) is reached, such that the clustering stops when the value of the difference of all reference spectra between two iterations is smaller than the value defined by *fuzzy abort*.

For the data evaluation of the current dataset (both IPR and background aerosol particles) a mixture of manual and automatic clustering was used. First, an automatic clustering was done with the parameters shown in Table A1.

The rest cluster, containing the cluster with all spectra that did not fulfill the given parameters, was first clustered automatically with a lower cluster difference (0.6) and the remaining spectra were sorted manually with a correlation factor $r^2 \geq 0.7$.

Acknowledgements. This work was supported by the DFG projects FOR 1525 (INUIT), SPP 1294 (HALO, grant Me 3524/1-2), the Max Planck Society, the European Union Seventh Framework Programme (FP7/2007-2013) under grant agreement no 2662254 (ACTRIS TNA) and the Swiss National Science Foundation (200021L 135356).

The authors gratefully acknowledge the NOAA Air Resources Laboratory (ARL) for the provision of the HYSPLIT transport and dispersion model and/or READY website (http://www.ready.noaa.gov) used in this publication.

We would like to thank Swiss Meteorological Institute (MeteoSwiss) for providing meteorological measurements and the International Foundation High Altitude Research Station Jungfraujoch and Gornergrat (HFSJG) for the opportunity to perform experiments at the Jungfraujoch. Additional thanks go to Oliver Appel (MPIC Mainz) for help with OPC error calculations, to Oliver Schlenczek (University Mainz) for cloud observations at the JFJ and to Udo Kästner (TROPOS) for his help during the measurements at the JFJ.

ACPD
15, 4677–4724, 2015

The service charges for this open-access publication have been covered by the Max Planck Society.

References

Abbatt, J. P., Benz, S., Cziczo, D. J., Kanji, Z., Lohmann, U., and Möhler, O.: Solid ammonium sulfate aerosols as ice nuclei: a pathway for cirrus cloud formation, Science, 313, 1770–1773, 2006.

Adler, G., Koop, T., Haspel, C., Taraniuk, I., Moise, T., Koren, I., Heiblum, R. H., and Rudich, Y.: Formation of highly porous aerosol particles by atmospheric freeze-drying in ice clouds, P. Natl. Acad. Sci. USA, 110, 20414–20419, 2013.

Atkinson, J. D., Murray, B. J., Woodhouse, M. T., Whale, T. F., Baustian, K. J., Carslaw, K. S., Dobbie, S., O'Sullivan, D., and Malkin, T. L.: The importance of feldspar for ice nucleation by mineral dust in mixed-phase clouds, Nature, 498, 355–358, 2013.

Bezdek, J. C., Ehrlich, R., and Full, W.: Fcm – the Fuzzy C-Means clustering-algorithm, Comput. Geosci., 10, 191–203, 1984.

Brands, M., Kamphus, M., Böttger, T., Schneider, J., Drewnick, F., Roth, A., Curtius, J., Voigt, C., Borbon, A., Beekmann, M., Bourdon, A., Perrin, T., and Borrmann, S.: Characterization of a newly developed aircraft-based laser ablation aerosol mass spectrometer (ALABAMA) and first field deployment in urban pollution plumes over Paris during MEGAPOLI 2009, Aerosol Sci. Tech., 45, 46–64, 2011.

Cantrell, W. and Heymsfield, A.: Production of ice in tropospheric clouds: a review, B. Am. Meteorol. Soc., 6, 795–807, 2005.

Chen, Y., Kreidenweis, S. M., McInnes, L. M., Rogers, D. C., and DeMott, P. J.: Single particle analyses of ice nucleating aerosols in the upper troposphere and lower stratosphere, Geophys. Res. Lett., 25, 1391–1394, 1998.

Chou, C., Stetzer, O., Weingartner, E., Jurányi, Z., Kanji, Z. A., and Lohmann, U.: Ice nuclei properties within a Saharan dust event at the Jungfraujoch in the Swiss Alps, Atmos. Chem. Phys., 11, 4725–4738, doi:10.5194/acp-11-4725-2011, 2011.

Corbin, J. C., Rehbein, P. J. G., Evans, G. J., and Abbatt, J. P. D.: Combustion particles as ice nuclei in an urban environment: evidence from single-particle mass spectrometry, Atmos. Environ., 51, 286–292, 2012.

Cozic, J., Mertes, S., Verheggen, B., Cziczo, D. J., Gallavardin, S. J., Walter, S., Baltensperger, U., and Weingartner, E.: Black carbon enrichment in atmospheric ice particle residuals observed in lower tropospheric mixed phase clouds, J. Geophys. Res., 113, D15209, doi:10.1029/2007JD009266, 2008a.

Cozic, J., Verheggen, B., Weingartner, E., Crosier, J., Bower, K. N., Flynn, M., Coe, H., Henning, S., Steinbacher, M., Henne, S., Collaud Coen, M., Petzold, A., and Baltensperger, U.: Chemical composition of free tropospheric aerosol for PM1 and coarse mode at the high alpine site Jungfraujoch, Atmos. Chem. Phys., 8, 407–423, doi:10.5194/acp-8-407-2008, 2008b.

Cziczo, D. J.: Observations of organic species and atmospheric ice formation, Geophys. Res. Lett., 31, L12116, doi:10.1029/2004GL019822, 2004.

Cziczo, D. J., DeMott, P. J., Brock, C., Hudson, P. K., Jesse, B., Kreidenweis, S. M., Prenni, A. J., Schreiner, J., Thomson, D. S., and Murphy, D. M.: A method for single particle mass spectrometry of ice nuclei, Aerosol Sci. Tech., 37, 460–470, 2003.

Cziczo, D. J., Murphy, D. M., Hudson, P. K., and Thomson, D. S.: Single particle measurements of the chemical composition of cirrus ice residue during CRYSTAL-FACE, J. Geophys. Res., 109, D04201, doi:10.1029/2004JD004964, 2004.

Cziczo, D. J., Stetzer, O., Worringen, A., Ebert, M., Weinbruch, S., Kamphus, M., Gallavardin, S. J., Curtius, J., Borrmann, S., Froyd, K. D., Mertes, S., Möhler, O., and Lohmann, U.: Inadvertent climate modification due to anthropogenic lead, Nat. Geosci., 2, 333–336, 2009.

Dall'Osto, M.: Characterization of individual airborne particles by using aerosol time-of-flight mass spectrometry at Mace Head, Ireland, J. Geophys. Res., 109, D21302, doi:10.1029/2004JD004747, 2004.

Dall'Osto, M. and Harrison, R.: Chemical characterisation of single airborne particles in Athens (Greece) by ATOFMS, Atmos. Environ., 40, 7614–7631, 2006.

Dall'Osto, M., Harrison, R. M., Highwood, E. J., O'Dowd, C., Ceburnis, D., Querol, X., and Achterberg, E. P.: Variation of the mixing state of Saharan dust particles with atmospheric transport, Atmos. Environ., 44, 3135–3146, 2010.

De Foy, B., Smyth, A. M., Thompson, S. L., Gross, D. S., Olson, M. R., Sager, N., and Schauer, J. J.: Sources of nickel, vanadium and black carbon in aerosols in Milwaukee, Atmos. Environ., 59, 294–301, 2012.

ACPD
15, 4677–4724, 2015

In-situ single submicron particle composition analysis of ice residuals

S. Schmidt et al.

CC BY

DeCarlo, P. F., Slowik, J. G., Worsnop, D. R., Davidovits, P., and Jimenez, J. L.: Particle morphology and density characterization by combined mobility and aerodynamic diameter measurements. Part. 1: Theory, Aerosol Sci. Tech., 38, 1185–1205, 2004.
DeMott, P. J.: African dust aerosols as atmospheric ice nuclei, Geophys. Res. Lett., 30, 1732, doi:10.1029/2003GL017410, 2003.
DeMott, P. J., Rogers, D. C., Kreidenweis, S. M., Chen, Y., Twohy, C. H., Baumgardner, D., Heymsfield, A. J., and Chan, K. R.: The role of heterogeneous freezing nucleation in upper tropospheric clouds: inferences from SUCCESS, Geophys. Res. Lett., 25, 1387–1390, 1998.
DeMott, P. J., Chen, Y., Kreidenweis, S. M., Rogers, D. C., and Sherman, D. E.: Ice formation by black carbon particles, Geophys. Res. Lett., 26, 2429–2432, 1999.
DeMott, P. J., Cziczo, D. J., Prenni, A. J., Murphy, D. M., Kreidenweis, S. M., Thomson, D. S., Borys, R., and Rogers, D. C.: Measurements of the concentration and composition of nuclei for cirrus formation, P. Natl. Acad. Sci. USA, 100, 14655–14660, 2003.
DeMott, P. J., Prenni, A. J., Liu, X., Kreidenweis, S. M., Petters, M. D., Twohy, C. H., Richardson, M. S., Eidhammer, T., and Rogers, D. C.: Predicting global atmospheric nuclei distributions and their impacts on climate, P. Natl. Acad. Sci. USA, 107, 11217–11222, 2010.
Diehl, K., Quick, C., Matthias-Maser, S., Mitra, S. K., and Jaenicke, R.: The ice nucleating ability of pollen Part I: Laboratory studies in deposition and condensation freezing mode, Atmos. Res., 58, 75–87, 2001.
Diehl, K. and Wurzler, S.: Air parcel model simulations of a convective cloud: bacteria acting as immersion ice nuclei, Atmos. Environ., 44, 4622–4628, 2010.
Diehl, K., Debertshäuser, M., Eppers, O., Schmithüsen, H., Mitra, S. K., and Borrmann, S.: Particle surface area dependence of mineral dust in immersion freezing mode: investigations with freely suspended drops in an acoustic levitator and a vertical wind tunnel, Atmos. Chem. Phys., 14, 12343–12355, doi:10.5194/acp-14-12343-2014, 2014.
Draxler, R. R. and Rolph, G. D.: HYSPLIT (HYbrid Single-Particle Lagrangian Integrated Trajectory) Model access via NOAA ARL READY Website, available at: http://ready.arl.noaa.gov/HYSPLIT.php (last access: 31 October 2014), NOAA Air Resources Laboratory, Silver Spring, MD, 2012.
Dymarska, M., Murray, B. J., Sun, L., Eastwood, M. L., Knopf, D. A., and Bertram, A. K.: Deposition ice nucleation on soot at temperatures relevant for the lower troposphere, J. Geophys. Res., 111, D04204, doi:10.1029/2005JD006627, 2006.

ACPD
15, 4677–4724, 2015

Ebert, M., Worringen, A., Benker, N., Mertes, S., Weingartner, E., and Weinbruch, S.: Chemical composition and mixing-state of ice residuals sampled within mixed phase clouds, Atmos. Chem. Phys., 11, 2805–2816, doi:10.5194/acp-11-2805-2011, 2011.

Fergenson, D. P., Pitesky, M. E., Tobias, H. J., Steele, P. T., Czerwieniec, G. A., Russell, S. C., Lebrilla, C. B., Horn, J. M., Coffee, K. R., Srivastava, A., Pillai, S. P., Shih, M.-T. P., Hall, H. L., Ramponi, A. J., Chang, J. T., Langlois, R. G., Estacio, P. L., Hadley, R. T., Frank, M., and Gard, E. E.: Reagentless detection and classification of individual bioaerosol particles in seconds, Anal. Chem., 76, 373–378, 2004.

Frank, M., Gard, E. E., Tobias, H. J., Adams, K. L., Bogan, M. J., Coffee, K. R., Farquar, G. R., Fergenson, D. P., Martin, S. I., Pitesky, M., Riot, V. J., Srivastava, A., Steele, P. T., and Williams, A. M.: Single-particle aerosol mass spectrometry (SPAMS) for high-throughput and rapid analysis of biological aerosols and single cells, ACS Symp. Ser., 1065, 161–196, doi:10.1021/bk-2011-1065.ch010, 2011.

Froyd, K. D., Murphy, D. M., Lawson, P., Baumgardner, D., and Herman, R. L.: Aerosols that form subvisible cirrus at the tropical tropopause, Atmos. Chem. Phys., 10, 209–218, doi:10.5194/acp-10-209-2010, 2010.

Gerber, H.: Microphysics of marine stratocumulus clouds with two drizzle modes, J. Atmos. Sci., 53, 1649–1662, 1996.

Hartmann, S., Niedermeier, D., Voigtländer, J., Clauss, T., Shaw, R. A., Wex, H., Kiselev, A., and Stratmann, F.: Homogeneous and heterogeneous ice nucleation at LACIS: operating principle and theoretical studies, Atmos. Chem. Phys., 11, 1753–1767, doi:10.5194/acp-11-1753-2011, 2011.

Hinz, K. P., Greweling, M., Drews, F., and Spengler, B.: Data processing in on-line laser mass spectrometry of inorganic, organic, or biological airborne particles, Am. Soc. Mass Spectrom., 10, 648–660, 1999.

Hoose, C. and Möhler, O.: Heterogeneous ice nucleation on atmospheric aerosols: a review of results from laboratory experiments, Atmos. Chem. Phys., 12, 9817–9854, doi:10.5194/acp-12-9817-2012, 2012.

Huang, M., Xia, Z. X., Wang, H. B., Zeng, Q. H., and Wang, Q.: The range of the value for the fuzzifier of the fuzzy c-means algorithm, Pattern Recogn. Lett., 33, 2280–2284, 2012.

Huang, M., Hao, L., Guo, X., Hu, C., Gu, X., Zhao, W., Wang, Z., Fang, L., and Zhang, W.: Characterization of secondary organic aerosol particles using aerosol laser time-of-flight mass spectrometer coupled with FCM clustering algorithm, Atmos. Environ., 64, 85–94, 2013.

ACPD
15, 4677–4724, 2015

Kamphus, M., Ettner-Mahl, M., Brands, M., Curtius, J., Drewnick, F., and Borrmann, S.: Comparison of two aerodynamic lenses as an inlet for a single particle laser ablation mass spectrometer, Aerosol Sci. Tech., 42, 970–980, 2008.

Kamphus, M., Ettner-Mahl, M., Klimach, T., Drewnick, F., Keller, L., Cziczo, D. J., Mertes, S., Borrmann, S., and Curtius, J.: Chemical composition of ambient aerosol, ice residues and cloud droplet residues in mixed-phase clouds: single particle analysis during the Cloud and Aerosol Characterization Experiment (CLACE 6), Atmos. Chem. Phys., 10, 8077–8095, doi:10.5194/acp-10-8077-2010, 2010.

Kandler, K., Lieke, K., Benker, N., Emmel, C., Küpper, M., Müller-Ebert, D., Ebert, M., Scheuvens, D., Schladitz, A., and Schütz, L.: Electron microscopy of particles collected at Praia, Cape Verde, during the Saharan Mineral Dust Experiment: particle chemistry, shape, mixing state and complex refractive index, Tellus B, 63, 475–496, 2011.

Klimach, T.: Chemische Zusammensetzung der Aerosole – Design und Datenauswertung eines Einzelpartikel-Laserablationsmassenspektrometers, Ph.D. thesis, University of Mainz, Mainz, Germany, 2012.

Koop, T., Luo, B. P., Tsias, A., and Peter, T.: Water activity as the determinant for homogeneous ice nucleation in aqueous solutions, Nature, 406, 611–614, 2000.

Kupiszewski, P., Weingartner, E., Vochezer, P., Bigi, A., Rosati, B., Gysel, M., Schnaiter, M., and Baltensperger, U.: The Ice Selective Inlet: a novel technique for exclusive extraction of pristine ice crystals in mixed-phase clouds, Atmos. Meas. Tech. Discuss., 7, 12481–12515, doi:10.5194/amtd-7-12481-2014, 2014.

Lance, S., Brock, C. A., Rogers, D., and Gordon, J. A.: Water droplet calibration of the Cloud Droplet Probe (CDP) and in-flight performance in liquid, ice and mixed-phase clouds during ARCPAC, Atmos. Meas. Tech., 3, 1683–1706, doi:10.5194/amt-3-1683-2010, 2010.

Liu, P., Ziemann, P. J., Kittelson, D. B., and McMurry, P. H.: Generating particle beams of controlled dimensions and divergence: I. Theory of particle motion in aerodynamic lenses and nozzle expansions, Aerosol Sci. Tech., 22, 293–313, 1995a.

Liu, P., Ziemann, P. J., Kittelson, D. B., and McMurry, P. H.: Generating particle beams of controlled dimensions and divergence: II. Experimental evaluation of particle motion in aerodynamic lenses and nozzle expansions, Aerosol Sci. Tech., 22, 314–324, 1995b.

Liu, P. S. K., Deng, R., Smith, K. A., Williams, L. R., Jayne, J. T., Canagaratna, M. R., Moore, K., Onasch, T. B., Worsnop, D. R., and Deshler, T.: Transmission efficiency of an aerodynamic

focusing lens system: comparison of model calculations and laboratory measurements for the aerodyne aerosol mass spectrometer, Aerosol Sci. Tech., 41, 721–733, 2007.
Lohmann, U. and Feichter, J.: Global indirect aerosol effects: a review, Atmos. Chem. Phys., 5, 715–737, doi:10.5194/acp-5-715-2005, 2005.
Mertes, S., Lehmann, K., Nowak, A., Massling, A., and Wiedensohler, A.: Link between aerosol hygroscopic growth and droplet activation observed for hill-capped clouds at connected flow conditions during FEBUKO, Atmos. Environ., 39, 4247–4256, 2005.
Mertes, S., Verheggen, B., Walter, S., Connolly, P., Ebert, M., Schneider, J., Bower, K. N., Cozic, J., Weinbruch, S., Baltensperger, U., and Weingartner, E.: Counterflow virtual impactor based collection of small ice particles in mixed-phase clouds for the physico-chemical characterization of tropospheric ice nuclei: sampler description and first case study, Aerosol Sci. Tech., 41, 848–864, 2007.
Möhler, O., DeMott, P. J., Vali, G., and Levin, Z.: Microbiology and atmospheric processes: the role of biological particles in cloud physics, Biogeosciences, 4, 1059–1071, doi:10.5194/bg-4-1059-2007, 2007.
Möhler, O., Georgakopoulos, D. G., Morris, C. E., Benz, S., Ebert, V., Hunsmann, S., Saathoff, H., Schnaiter, M., and Wagner, R.: Heterogeneous ice nucleation activity of bacteria: new laboratory experiments at simulated cloud conditions, Biogeosciences, 5, 1425–1435, doi:10.5194/bg-5-1425-2008, 2008.
Murphy, D. M., Hudson, P. K., Cziczo, D. J., Gallavardin, S., Froyd, K. D., Johnston, M. V., Middlebrook, A. M., Reinard, M. S., Thomson, D. S., Thornberry, T., and Wexler, A. S.: Distribution of lead in single atmospheric particles, Atmos. Chem. Phys., 7, 3195–3210, doi:10.5194/acp-7-3195-2007, 2007.
Murray, B. J., Wilson, T. W., Dobbie, S., Cui, Z., Al-Jumur, S. M. R. K., Möhler, O., Schnaiter, M., Wagner, R., Benz, S., Niemand, M., Saathoff, H., Ebert, V., Wagner, S., and Kärcher, B.: Heterogeneous nucleation of ice particles on glassy aerosols under cirrus conditions, Nat. Geosci., 3, 233–237, 2010.
Murray, B. J., Broadley, S. L., Wilson, T. W., Atkinson, J. D., and Wills, R. H.: Heterogeneous freezing of water droplets containing kaolinite particles, Atmos. Chem. Phys., 11, 4191–4207, doi:10.5194/acp-11-4191-2011, 2011.
Murray, B. J., O'Sullivan, D., Atkinson, J. D., and Webb, M. E.: Ice nucleation by particles immersed in supercooled cloud droplets, Chem. Soc. Rev., 41, 6519–6554, 2012.

ACPD
15, 4677–4724, 2015

Pratt, K. A. and Prather, K. A.: Aircraft measurements of vertical profiles of aerosol mixing states, J. Geophys. Res., 115, D11305, doi:10.1029/2009JD013150, 2010.
Pratt, K. A., DeMott, P. J., French, J. R., Wang, Z., Westphal, D. L., Heymsfield, A. J., Twohy, C. H., Prenni, A. J., and Prather, K. A.: In situ detection of biological particles in cloud ice-crystals, Nat. Geosci., 2, 398–401, 2009.
Pratt, K. A., Heymsfield, A. J., Twohy, C. H., Murphy, S. M., DeMott, P. J., Hudson, J. G., Subramanian, R., Wang, Z., Seinfeld, J. H., and Prather, K. A.: In situ chemical characterization of aged biomass-burning aerosols impacting cold wave clouds, J. Atmos. Sci., 67, 2451–2468, 2010.
Prenni, A. J., Petters, M. D., Kreidenweis, S. M., Heald, C. L., Martin, S. T., Artaxo, P., Garland, R. M., Wollny, A. G., and Pöschl, U.: Relative roles of biogenic emissions and Saharan dust as ice nuclei in the Amazon basin, Nat. Geosci., 2, 402–405, 2009.
Pruppacher, H. R. and Klett, J. D.: Microphysics of Clouds and Precipitation, Kluwer Acedemic Publishers, Dodrecht, 2010.
Rogers, D. C., DeMott, P. J., Kreidenweis, S. M., and Chen, Y. L.: Measurements of ice nucleating aerosols during SUCCESS, Geophys. Res. Lett., 25, 1383–1386, 1998.
Rolph, G. D.: Real-time Environmental Applications and Display sYstems (READY) Website (http://ready.arl.noaa.gov), NOAA Air Resources Laboratory, Silver Spring, MD, 2014.
Roth, A.: Untersuchungen von Aerosolpartikeln und Wolkenresidualpartikeln mittels Einzelpartikel-Massenspektrometrie und optischen Methoden, Ph.D. thesis, University of Mainz, Mainz, Germany, 2014.
Seinfeld, J. H. and Pandis, S. N.: Atmospheric Chemistry and Physics: From Air Pollution to Climate Change, John Wiley and Sons, Inc., New York, 2006.
Steinke, I., Hoose, C., Möhler, O., Connolly, P., and Leisner, T.: A new temperature and humidity dependent surface site density approach for deposition ice nucleation, Atmos. Chem. Phys. Discuss., 14, 18499–18539, doi:10.5194/acpd-14-18499-2014, 2014.
Trimborn, A.: Online analysis of atmospheric particles with a transportable laser mass spectrometer during LACE 98, J. Geophys. Res., 107, 8132, doi:10.1029/2001JD000590, 2002.
Twohy, C. H., DeMott, P. J., Pratt, K. A., Subramanian, R., Kok, G. L., Murphy, S. M., Lersch, T., Heymsfield, A. J., Wang, Z., Prather, K. A., and Seinfeld, J. H.: Relationships of biomass-burning aerosols to ice in orographic wave clouds, J. Atmos. Sci., 67, 2437–2450, 2010.
Vali, G.: Repeatability and randomness in heterogeneous freezing nucleation, Atmos. Chem. Phys., 8, 5017–5031, doi:10.5194/acp-8-5017-2008, 2008.

ACPD
15, 4677–4724, 2015

CC BY

von Blohn, N., Mitra, S. K., Diehl, K., and Borrmann, S.: The ice nucleating ability of pollen, Atmos. Res., 78, 182–189, 2005.

von der Weiden, S.-L., Drewnick, F., and Borrmann, S.: Particle Loss Calculator – a new software tool for the assessment of the performance of aerosol inlet systems, Atmos. Meas. Tech., 2, 479–494, doi:10.5194/amt-2-479-2009, 2009.

Weingartner, E., Nyeki, S., and Baltensperger, U.: Seasonal and diurnal variation of aerosol size distributions ($10 < D < 750$ nm) at a high-alpine site (Jungfraujoch 3580 m a.s.l.), J. Geophys. Res., 104, 26809–26820, 1999.

Wendisch, M.: A quantitative comparison of ground-based FSSP and PVM measurements, B. Am. Meteorol. Soc., 15, 887–900, 1998.

Wise, M. E., Baustian, K. J., Koop, T., Freedman, M. A., Jensen, E. J., and Tolbert, M. A.: Depositional ice nucleation onto crystalline hydrated NaCl particles: a new mechanism for ice formation in the troposphere, Atmos. Chem. Phys., 12, 1121–1134, doi:10.5194/acp-12-1121-2012, 2012.

Worringen, A., Kandler, K., Benker, N., Dirsch, T., Weinbruch, S., Mertes, S., Schenk, L., Kästner, U., Frank, F., Nillius, B., Bundke, U., Rose, D., Curtius, J., Kupiszewski, P., Weingartner, E., Schneider, J., Schmidt, S., and Ebert, M.: Single-particle characterization of ice-nucleating particles and ice particle residuals sampled by three different techniques, Atmos. Chem. Phys. Discuss., 14, 23027–23073, doi:10.5194/acpd-14-23027-2014, 2014.

ACPD
15, 4677–4724, 2015

In-situ single submicron particle composition analysis of ice residuals

S. Schmidt et al.

Table 1. Date and time of the cloud events during which measurements were taken behind Ice-CVI or ISI, along with the number of the measured spectra, the evaluation of the Ice-CVI-events and the weather conditions and cloud formation during these events. The times of each cloud event based (a) on the particle counter operated behind the Ice-CVI or (b) on the liquid water content measured by two PVM instruments and a CDP outside the laboratory.

Event	Cloud event (LT)	Inlet	Number of number spectra	Evaluation of the Ice CVI-events	Weather conditions and clouds
1	[a]22 Jan 2013 02:00–13:05	CVI	174	++	Warm front occlusive low pressure system
2	[a]27 Jan 2013 15:30–28 Jan 2013 10:30	CVI	78	++	Occlusive frontal system, Ns
3	[a]29 Jan 2013 01:30–23:00	CVI	23	++	Unstable warm front; first Ns than Cb
4	[a]30 Jan 2013 16:00–31 Jan 2013 01:00	CVI	39	++	Squall line at cold front; Cb
5	[a,b]31 Jan 2013 17:30–3 Feb 2013 11:00	ISI/CVI	27 (ISI) 1117 (CVI)	+−	31 Jan: cellular convection; Cu 1–2 Feb: frontal wave; Ns and Cb Until 3 Feb cellular convection; Cb
6	[a]5 Feb 2013 14:45–6 Feb 2013 05:06	CVI	69	+−	Squall line at postfrontal convergence line; Cb
7	[a]6 Feb 2013 08:30–8 Feb 2013 12:50	CVI	97	+−	6 Feb: Convective dominating low-pressure vortex; Cb From 7 Feb on: cellular convection; Cu
8	[a]8 Feb 2013 22:30–9 Feb 2013 19:00	CVI	44	+−	Diamond dust and cellular convection at convergence line; Ci, Cu (Cb)
9	[a]10 Feb 2013 16:00–23:50	CVI	2	++	Approaching warm front; Ci, Cs, As
10	[a]11 Feb 2013 06:20–12 Feb 2013 06:30	CVI	12	++	Warm front; Ns
11	[a]12 Feb 2013 16:00–13 Feb 2013 01:20	CVI	8	+−	Back of a low with northeast stream; Ns, Ac, As
12	[b]14 Feb 2013 16:00–16 Feb 2013 01:05	ISI	114		Low pressure system; As, Cu, Cb, Ac
13	[a]19 Feb 2013 15:00–20 Feb 2013 19:05	CVI	1	++	Cold front from North; Ac, Ns, Sc, Cu
14	[b]24 Feb 2013 02:00–25 Feb 2013 18:40	ISI	3		Approaching warm front with precipitation; Cs, As, Ns

Ac: altocumulus; As: altostratus; Cb: cumulonimbus; Ci: cirrus; Cs: cirrostratus; Cu: cumulus; Ns: nimbostratus; Sc: stratocumulus.

ACPD
15, 4677–4724, 2015

CC BY

Table A1. Chosen clustering parameter.

Preprocessing type	Power each m/z
Preprocessing power	0.5
Normalization type	Sum
Cluster difference	0.7 (0.6)
Distance	Correlation
Fuzzifier	1.2
Fuzzy abort	0.0001

ACPD
15, 4677–4724, 2015

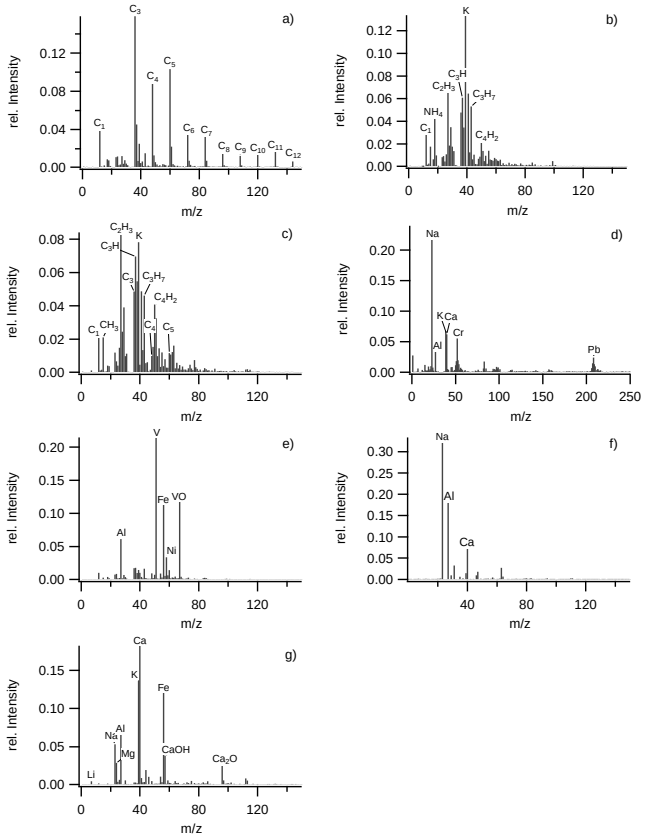

Figure 1. Average mass spectra of each particle type. **(a)** black carbon; **(b)** organic carbon; **(c)** black carbon internally mixed with organic carbon; **(d)** lead containing particles; **(e)** industrial metals; **(f)** BioMinSal; **(g)** minerals.

ACPD
15, 4677–4724, 2015

CC BY

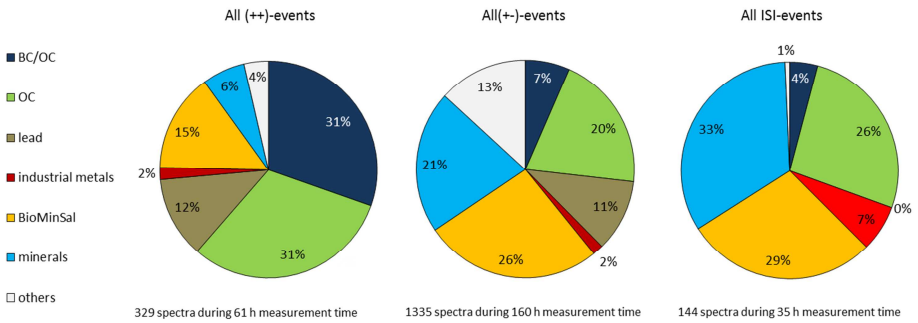

Figure 2. Results of the IPR composition analysis. Left and middle: measurements behind the Ice-CVI (left: all (++)-events; middle: all (+−)-events). Right: IPR composition measured behind the ISI.

ACPD
15, 4677–4724, 2015

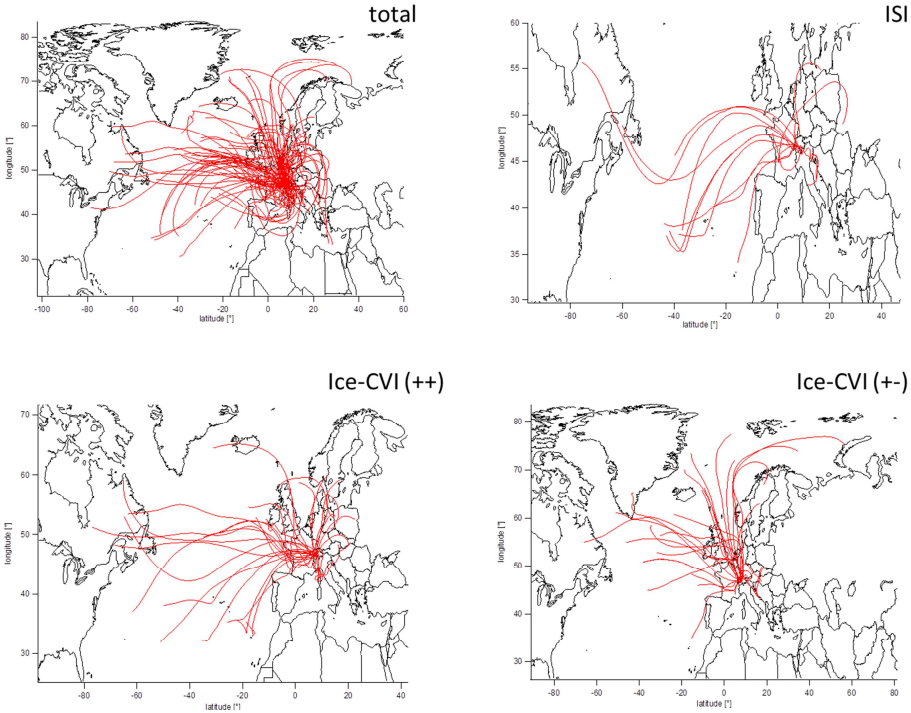

Figure 3. 72 h backward trajectories calculated with CRISP/HYSPLIT (one trajectory every 6 h).

ACPD
15, 4677–4724, 2015

In-situ single submicron particle composition analysis of ice residuals

S. Schmidt et al.

CC BY

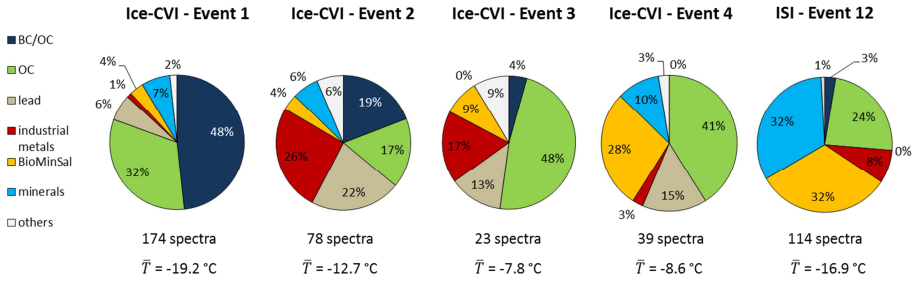

Figure 4. Comparison of the composition analysis of five events measuring behind the Ice-CVI (all (++)-events, Event 1: 22 January 2013 02:00–13:05; Event 2: 27 January 2013 15:30–28 January 2013 10:30; Event 3: 29 January 2013 01:30–23:00 and Event 4: 30 January 2013 16:00–31 January 2013 01:00) and the ISI (Event 12: 14 February 2013 18:10–16 February 2013 01:05) together with the corresponding average temperature during each event.

ACPD
15, 4677–4724, 2015

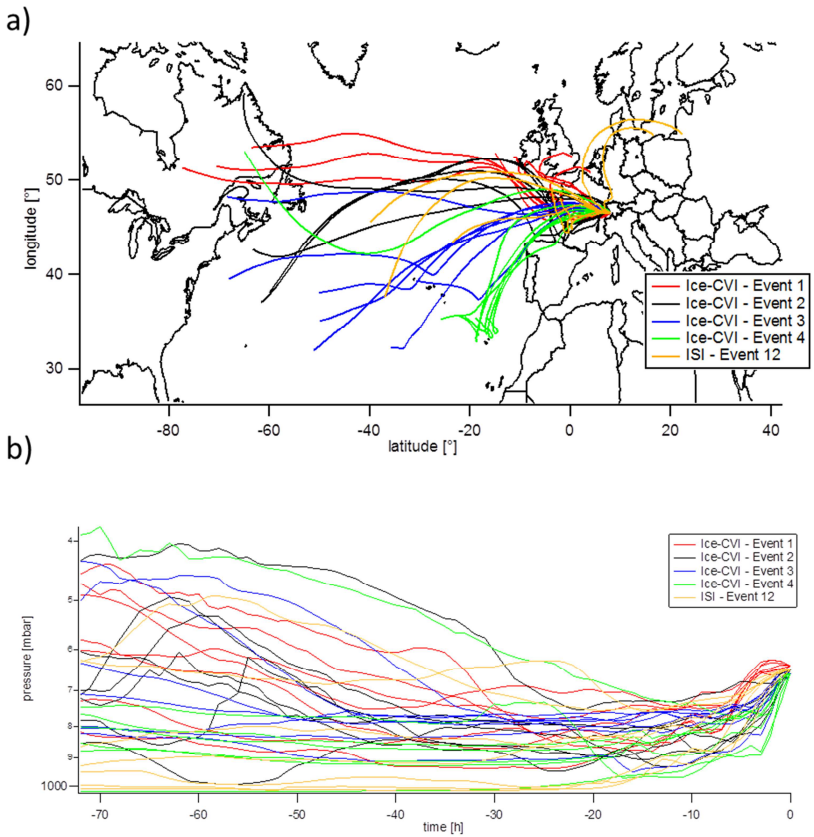

Figure 5. (a) 72 h backward trajectories (one trajectory every three hours) calculated with CRISP for each event. **(b)** The altitudes of air masses reaching the Jungfraujoch as a function of time, converted to pressure units.

ACPD
15, 4677–4724, 2015

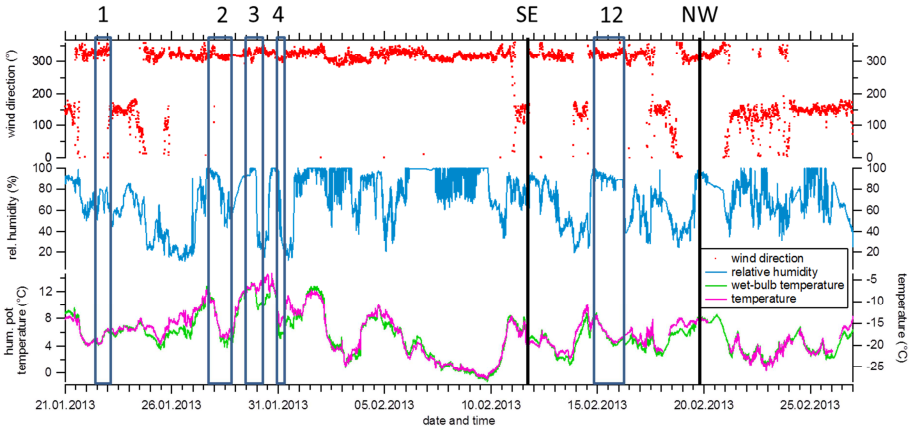

Figure 6. Wind direction, relative humidity, potential wet-bulb temperature and temperature over the whole measurement period (data from MeteoSwiss at the JFJ station). Black lines denote the events with different air mass origin. Events highlighted with blue bars denote the 5 different events from Sect. 2.1.1.

ACPD
15, 4677–4724, 2015

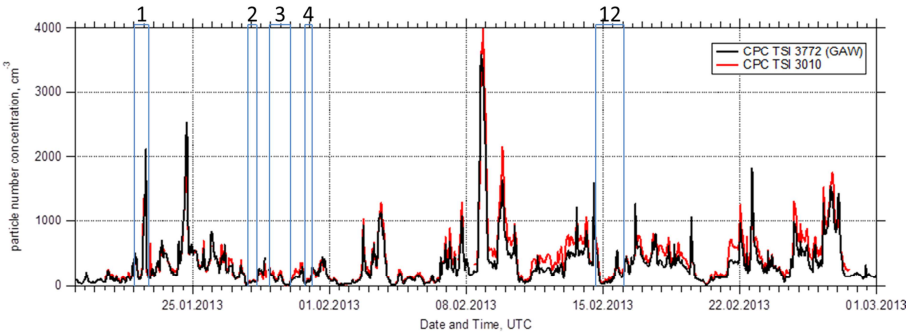

Figure 7. Particle number concentrations measured during the INUIT-JFJ/CLACE 2013 campaign by two different condensation particle counters (CPC): the GAW-CPC which is located directly behind the total inlet, and a TSI 3010 that was operated with a much longer sampling line (approx. 7 m) next to one of the aerosol mass spectrometers. Short elevated concentrations indicate local emissions. Events highlighted with blue bars denote the 5 different events from Sect. 2.1.1.

ACPD
15, 4677–4724, 2015

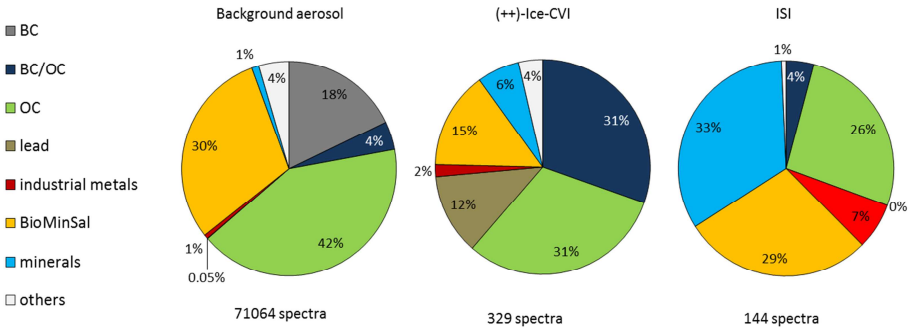

Figure 8. Comparison between the chemical composition of background aerosol particles (left) and IPR measured behind Ice-CVI (middle) and ISI (right).

ACPD
15, 4677–4724, 2015

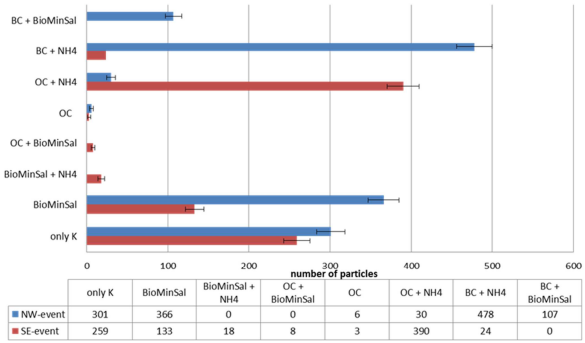

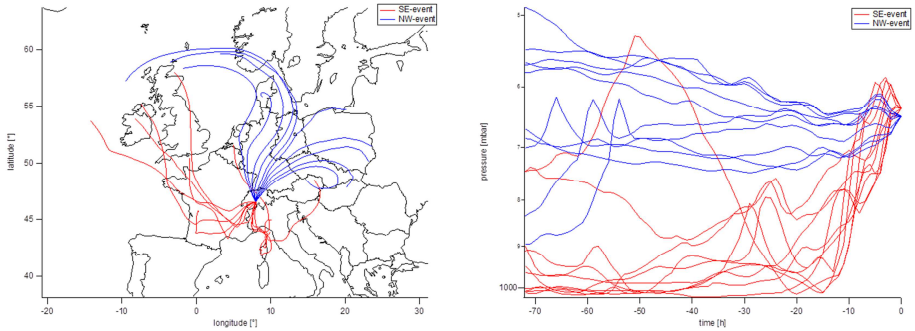

Figure 9. Comparison of two events measured during non-cloud episodes. The northwestern event (NW; blue) was on 19 February 2013 14:00–16:14 and the southeastern event (SE; red) was on 11 February 2013 10:32–14:27. 72 h back trajectories were calculated with one trajectory every 2 h.

ACPD
15, 4677–4724, 2015

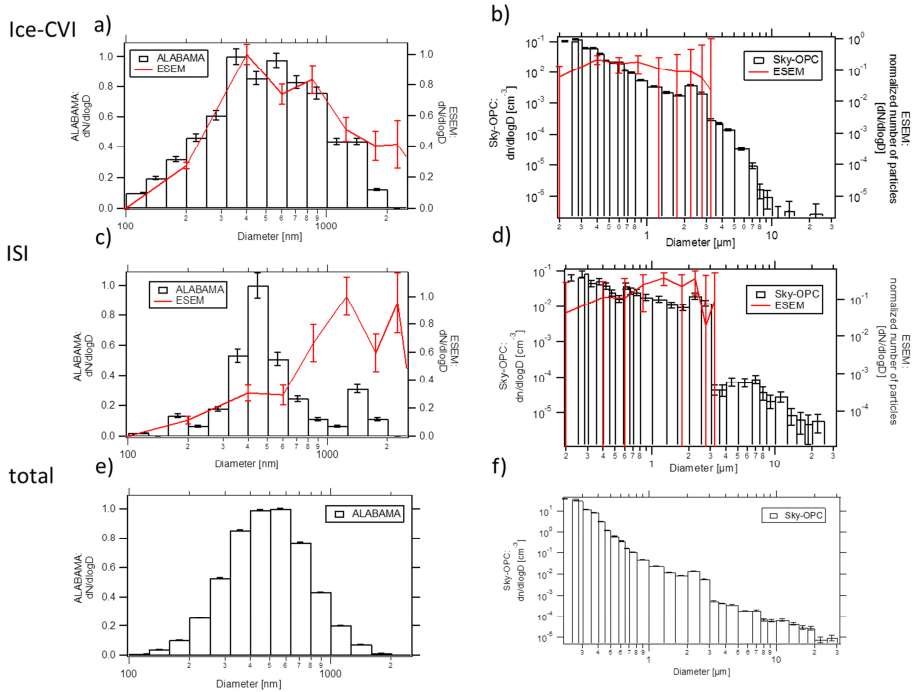

Figure 10. Measured size distribution of the IPR and background aerosol particles with the ALABAMA (bars; **a**, **c**, **e**) and Sky-OPC (bars; **b**, **d**, **f**) compared with the off-line SEM analysis of IPR samples (line; **a–d**). The error bars for the ALABAMA data result from counting statistics (averaged errors; $\Delta_{\text{Ice-CVI}} = 5.5\,\%$; $\Delta_{\text{ISI}} = 8.3\,\%$; $\Delta_{\text{total}} = 4\,\%$). The error of the OPC data results from Gaussian propagation of uncertainty, including counting statistics, the manufacturer-given error of the OPC of 3 %, and the error of the enrichment factor (4 % for the Ice-CVI and 20 % for the ISI). The error of the ESEM dataset was determined by counting statistics. Note the different axis scaling. The *y* axis is linear in **(a, c, e)** and logarithmic in **(b, d, f)**. The *x* axis range is 100–2500 nm in **(a, c, e)** and 200 nm–3 µm in **(b, d, f)**.

ACPD
15, 4677–4724, 2015

In-situ single submicron particle composition analysis of ice residuals

S. Schmidt et al.

CC BY

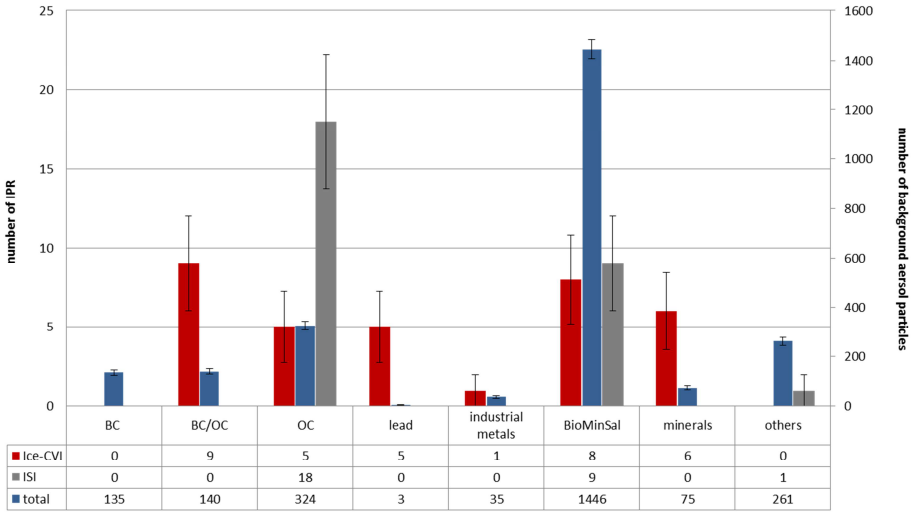

Figure 11. Chemical composition of IPR and background aerosol particles larger than 1000 nm measured behind the Ice-CVI (red), ISI (grey) and total inlet (blue). The error bars results from counting statistics.

ACPD
15, 4677–4724, 2015